

Electronic structure, electron transport properties, and relative stability of icosahedral quasicrystals and their 1/1 and 2/1 approximants in the Al-Mg-Zn alloy system

Tsunehiro Takeuchi and Uichiro Mizutani

Department of Crystalline Materials Science, Nagoya University, Furo-cho, Chikusa-ku, Nagoya 464-01, Japan

(Received 28 March 1995)

Electronic properties of icosahedral quasicrystals have been often discussed on the basis of the valence band structure of their cubic 1/1 approximants for which the band calculations are available. However, there exists no *a priori* justification for the neglect of the difference between the quasicrystal and its lowest-order approximant. Studies of the hierarchy dependence of the electronic structure and electron transport properties in a given system are, therefore, highly important. The Al-Mg-Zn system is chosen in this work, since a thermally stable quasicrystal and its 2/1 and 1/1 approximants can be prepared. Electronic properties, which include x-ray photoemission spectroscopy and soft x-ray spectroscopy valence band structure, the electronic specific heat coefficient, the resistivity, and the Hall coefficient, have been measured. We conclude that the electronic structure and electron transport properties of the thermally stable quasicrystal are substantially different from those of the 1/1 approximant but are essentially identical to those of the 2/1 approximant. It is also shown that the thermally stable icosahedral quasicrystal, the 2/1 and 1/1 approximants are competing among them as the Hume-Rothery electron phases, in which an electron concentration e/a and a composition ratio $x_{\text{Mg}}/(x_{\text{Al}} + x_{\text{Zn}})$ of a larger Mg atom over smaller Al and Zn atoms serve as two critical factors to decide their most stable compositions.

I. INTRODUCTION

Since the discovery of quasicrystals,¹ substantial progress has been made in deepening the understanding of quasiperiodic atomic structure and its effect on electronic structure and electron transport properties.² It has been now well established that the three-dimensional Penrose lattice forms the basis for the icosahedral quasicrystals and can be constructed by projecting a "strip" of a six-dimensional hypercube lattice onto a three-dimensional physical space.³ The strip orientation is chosen such that an icosahedral basis can be formed in the physical space. The rational approximant of the quasilattice is also constructed, if the golden mean $\tau = (1 + \sqrt{5})/2$ associated with the strip orientation for the icosahedral basis is replaced by a rational ratio $\tau_n = F_{n+1}/F_n$, where F_n is the Fibonacci number [$\tau_1 = \frac{1}{1}$, $\tau_2 = \frac{2}{1}$, $\tau_3 = \frac{3}{2}$, $\tau_4 = \frac{5}{3}$, \dots , $\tau_\infty = (1 + \sqrt{5})/2$].

Icosahedral quasicrystals are often divided into two families, depending on the structural unit in building up the quasiperiodic three-dimensional Penrose tiling. The Mackay-icosahedral-type quasicrystal possesses as its $\frac{1}{1}$ periodic cubic Penrose lattice (hereafter referred to as the 1/1 approximant) the atomic structure of the α -Al-Mn-Si with 136 atoms in its unit cell.^{4,5} As a second family, the triacontahedron-type quasicrystal possesses as the 1/1 approximant that of the Frank-Kasper or *R* phase with 162 or 160 atoms in the unit cell.^{6,7} Included in the former are quasicrystals like Al-Mn-Si, Al-Cu-Fe, Al-Pd-Re, and so on. The valence band structure in this family is dominated by *d*-electron states of the transition-metal elements involved. The quasicrystals in the latter are com-

posed of only simple elements like Al-Mg-Zn and Al-Li-Cu without containing transition-metal elements. Hence, the valence band near the Fermi level E_F is dominated by *sp* electrons.

As mentioned above, the Frank-Kasper phase (Al,Zn)₄₉Mg₃₂, the crystal structure of which had been determined in 1957 (Ref. 8) much earlier than the discovery of the quasicrystal, is now recognized as the 1/1 approximant to the icosahedral quasicrystal. Indeed, the discovery of the Al-Mg-Zn quasicrystal in 1985 has been guided by the presence of the Frank-Kasper phase in its phase diagram.⁹ Since then, the Al-Mg-Zn quasicrystal had been thought to be formed only as a metastable phase.¹⁰⁻¹² However, Takeuchi and co-workers¹³⁻¹⁵ recently discovered that the thermally stable quasicrystal can be formed in a very narrow composition range centered at Al₁₅Mg₄₄Zn₄₁.

The band calculation for the quasicrystal is not feasible, since its unit cell is infinitely large. Hence, the valence band structure for the quasicrystal has been conjectured from the calculations for the lowest-order approximants like 1/1 Al-Mn-Si (Ref. 5) and 1/1 Al-Li-Cu approximant.⁷ All these calculations showed the pseudogap formed close to the Fermi level E_F . These band calculations have been considered to be consistent with the density of states minimum at E_F deduced from the electronic specific heat¹⁶ as well as from spectroscopic measurements like x-ray photoemission spectroscopy (XPS) and soft x-ray spectroscopy¹⁷ (SXS) for thermally stable quasicrystals.

Certainly, the x-ray-diffraction spectra approach those of the quasicrystal with increasing the order of the ap-

proximant. Indeed, the x-ray-diffraction spectrum of the 2/1 approximant is already quite close to that of the quasicrystal.¹⁸ However, the structural resemblance with the quasicrystal is rather poor for the 1/1 approximant. A splitting of the diffraction lines in the 1/1 approximant is substantial, resulting in the appearance of major diffraction lines at scattering angles quite different from those of the quasicrystal.¹⁴ Hence, the resulting Brillouin zone of the 1/1 approximant differs critically from that of the thermally stable quasicrystal and this difference most likely results in the stabilization of these two phases at different electron concentrations in a given alloy system. Therefore, some caution should be exercised, when the electronic structure of the quasicrystal is discussed on the basis of the calculated band structure for the 1/1 approximant.

One may naturally think that the atomic structure and the related physical properties gradually approach that of the quasicrystal, as the order n of the approximant increases to an infinity corresponding to the quasicrystal. The n dependence of the electronic structure as well as the electron transport properties have been experimentally studied for the $(\text{Al}_x\text{Ga}_{1-x})_{20.5}\text{Zn}_{40.0}\text{Mg}_{39.5}$ system, where the thermally stable quasicrystal, 3/2-2/1-2/1, 2/1-2/1-2/1, and 1/1-1/1-1/1 approximants were successively formed over the entire Al concentration range x $0 \leq x \leq 1$.^{19,20} It was shown that the resistivity of the higher-order approximants is comparable to that of the quasicrystal, whereas that of the 1/1 approximant is 60–70% lower. Unfortunately, however, the electron concentration remains constant when x is varied in this system. Hence, no decisive conclusion was drawn as to whether the x dependence of various physical properties reflects the electronic effect through the Fermi surface-Brillouin zone interaction in this quaternary system.

The band calculation has been extended to higher-order approximants up to the 5/3 approximant in the Al-Mg-Zn (Ref. 21) and even the 8/5 approximant in the Al-Li-Cu.²² Hafner and Krajci²¹ calculated the valence band structure for the 1/1, 2/1, 3/2, and 5/3 approximants with the composition $\text{Al}_{16}\text{Mg}_{39.5}\text{Zn}_{44.5}$ and showed that the pseudogap appears at E_F for all approximants including the 1/1 approximant. Its depth is almost the same, regardless of the order of the approximants. They ascribed a failure of finding the hierarchy dependence of the pseudogap to the absence of a thermally stable quasicrystal in this system. As mentioned above, however, a thermally stable quasicrystal *does* exist in the Al-Mg-Zn system.

We consider that a systematic study of the electron concentration dependence of electronic properties in the icosahedral quasicrystal and its approximants would manifest their own characteristic features, since the difference in the Brillouin zone is not negligible. The Al-Mg-Zn system is well studied for this purpose. Three questions are addressed in this report. First, we present the XPS and SXS valence band structure for the 1/1, 2/1 approximants and icosahedral quasicrystals to establish the hierarchy dependence of the valence band structure. Second, a comparison of the electron transport properties is made among these three phases. Third, we discuss rel-

ative stability and point out that the compositions, at which a thermally stable quasicrystal, the 2/1, and 1/1 approximants are stabilized, can be understood by taking into account both an electronic energy gain and the atomic size factor expressed by the composition ratio for a larger Mg and smaller Al and Zn atoms.

II. EXPERIMENTAL PROCEDURE AND SAMPLE PREPARATION

Alloy ingots were prepared by induction melting of appropriate amounts of constituent elements 99.99% Al, 99.9% Mg, and 99.99% Zn in a boron-nitride crucible under Ar pressurized atmosphere. Ribbon specimens were fabricated by melt spinning onto a copper wheel at a tangential speed of 52 m/sec. The structure of as-quenched ribbons and those after heat treatments were studied by x-ray diffraction with Cu $K\alpha$ radiation. The composition was analyzed for representative samples by using inductively coupled plasma photoemission (ICP) spectroscopy. It agreed well with the nominal composition within $\pm 1\%$. Hence, the nominal composition is employed to calculate the electron per atom ratio, e/a , in the following discussions.

Two series (*A*) and (*B*) of samples were prepared. They are shown in Fig. 1 in the Al-Mg-Zn phase diagram. A first series (*A*) of samples was chosen as those having the compositions $\text{Al}_{60.5-x}\text{Mg}_{39.5}\text{Zn}_x$ ($x = 10.5, 15.5, 20.5, 25.5, 30.5, 35.5, \text{ and } 40.5$). All these samples after melt spinning turned out to be a mixture of the quasicrystal and the 1/1 approximant but crystallized into the 1/1 approximant single phase by annealing at 300°C for 5 h.

Another series of samples (*B*) marked as open circle, double circle, star, and solid triangle in the inset of Fig. 1 consists of a total of 19 samples expressed as $\text{Al}_x\text{Mg}_{44}\text{Zn}_{56-x}$ ($x = 13, 15, 20, 25$) and others including $\text{Al}_{15}\text{Mg}_{43}\text{Zn}_{42}$ and $\text{Al}_{15}\text{Mg}_{45}\text{Zn}_{40}$. A quasicrystalline single phase was formed by melt spinning for samples marked by open symbols (\circ , \odot , and \star), though the diffraction linewidth was rather broad. Their thermal stability was studied, using the differential scanning calorimeter with a heating rate of 10°C/min. Most samples crystallized into a mixture of the quasicrystal, the 1/1 approximant and other crystalline phases by evolving a very small exothermic heat upon crystallization at about 230°C.¹¹ However, the samples in the very vicinity of $\text{Al}_{15}\text{Mg}_{44}\text{Zn}_{41}$ accompanied two successive endothermic reactions at about 380 and 450°C in the differential scanning calorimetry. The occurrence of the endothermic reaction suggests that the quasicrystalline phase decomposes into liquid and the remaining phase as a result of the peritectic reaction. In other words, the quasicrystalline phase remains stable up to its melting point and, hence, we call it a thermally stable quasicrystal.^{13–15} Indeed, the $\text{Al}_{15}\text{Mg}_{44}\text{Zn}_{41}$ sample could maintain the quasicrystalline single phase even after prolonged annealing exceeding 5 h at 360°C and improve substantially its quasicrystallinity.

The $\text{Al}_{15}\text{Mg}_{43}\text{Zn}_{42}$ sample transformed into a 2/1 approximant single phase by annealing at 360°C for 1 h.

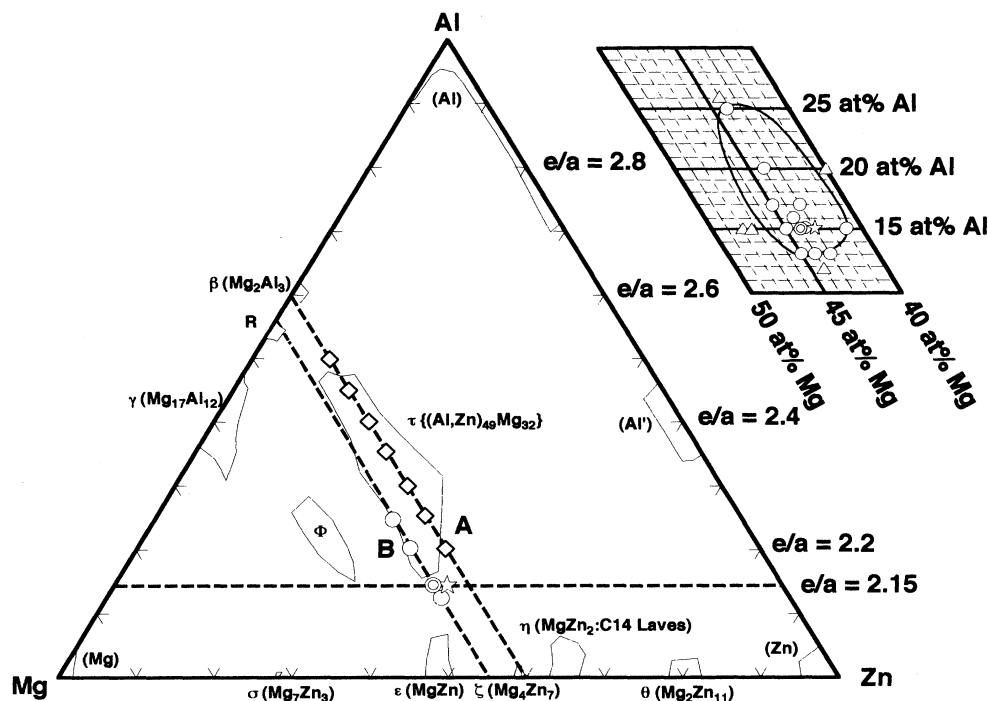


FIG. 1. Present samples in the Al-Mg-Zn alloy system. (A): $\text{Al}_{60.5-x}\text{Mg}_{39.5}\text{Zn}_x$ ($x = 10.5, 15.5, 20.5, 25.5, 30.5, 35.5,$ and 40.5). (B): $\text{Al}_x\text{Mg}_{44}\text{Zn}_{56-x}$ ($x = 13, 15, 16, 20, 25$) and others. All samples in the B series are shown in the inset. Symbols \circ , \odot , and \star in the inset represent a quasicrystalline single phase after melt spinning, but solid triangles (\blacktriangle) a mixture of a quasicrystalline phase and other phase(s). Physical properties were measured on samples shown in the main figure: the 1/1 approximant (\diamond), as-quenched metastable quasicrystal (\circ), a thermally stable icosahedral quasicrystal (\odot), and 2/1 approximant (\star). The $\tau\{(\text{Al,Zn})_{49}\text{Mg}_{32}\}$ refer to the 1/1 approximant. The phase diagram is reproduced from Ref. 27.

But the $\text{Al}_{15}\text{Mg}_{45}\text{Zn}_{40}$ sample precipitated a small amount of the hcp Mg phase in the quasicrystalline matrix under the same annealing condition. Similar studies have been done for all other samples in the vicinity of $\text{Al}_{15}\text{Mg}_{44}\text{Zn}_{41}$. By taking all these data into account, we conclude that the thermally stable icosahedral quasicrystal and 2/1 approximant are formed as a single phase at the compositions $\text{Al}_{15}\text{Mg}_{44}\text{Zn}_{41}$ and $\text{Al}_{15}\text{Mg}_{43}\text{Zn}_{42}$, respectively.

The XPS valence band spectra were measured using an Al $K\alpha$ monochromated x-ray beam (Surface Science Instrument, X-probe). The Al $K\beta$ (Al $3p$ distribution; valence band $\rightarrow 1s$) and Mg $K\beta$ (Mg $3p$ electrons, valence

band $\rightarrow 1s$) soft x-ray emissions were measured (Shimadzu, EPMA 8705). The energy scale relative to the Fermi level in the SXS spectra is determined within ± 0.2 eV by measuring the binding energy of the Al $2p_{3/2}$ and Mg $2p_{3/2}$ core levels and also the Al $K\alpha$ ($2p_{3/2} \rightarrow 1s$) emission lines.

The low-temperature specific heats were measured in the range 1.6–6 K and the electrical resistivity in the range 2–300 K. The Hall coefficient was also measured at 300 K with the use of the four-probe dc method. The details were described elsewhere.²³ Numerical data are summarized in Table I.

TABLE I. Physical properties of icosahedral quasicrystal, 1/1 approximant crystal, and 2/1 approximant crystal in the Mg-Al-Zn alloy system.

	Mg	Al	Zn	e/a	a (Å)	a_R (Å)	Density (g/cm ³)	γ (mJ/mol K ²)	γ_F	Θ_D (K)	$\rho_{300\text{K}}$ ($\mu\Omega$ cm)	$\rho_{2\text{K}}/\rho_{300\text{K}}$	R_H (10^{-11} m ³ /Å s)
1/1 phase	39.5	50.5	10	2.505	14.39	5.23±0.02	2.69	1.48±0.01	0.918	329.3±2.6	38		-9.3±0.9
	39.5	45.5	15	2.455	14.45	5.25±0.04	2.83	1.33±0.01	0.919	346.4±3.7	44	0.835	-12.1±1.2
	39.5	40.5	20	2.405	14.34	5.21±0.01	3.07	1.11±0.02	0.899	368.9±5.7	44	0.813	-16.9±1.7
	39.5	35.5	25	2.355	14.24	5.17±0.02	3.31	1.07±0.01	0.880	373.8±3.9	52	0.843	-28.2±2.8
	39.5	30.5	30	2.305	14.19	5.16±0.03	3.53	1.13±0.01	0.868	388.0±2.5	67	0.906	-35.7±3.6
	39.5	25.5	35	2.255	14.19	5.16±0.02	3.71	1.06±0.01	0.862	380.6±4.8	73	0.872	-39.7±4.0
	39.5	20.5	40	2.205	14.13	5.13±0.02	3.94	1.04±0.01	0.848	358.7±3.4	76	0.835	-35.9±3.6
I phase	44	25	31	2.250		5.19±0.10	3.48	0.99±0.01	0.873	325.7±2.4	92		-15.3±1.5
	44	20	36	2.200		5.22±0.06	3.70	0.92±0.02	0.860	335.2±3.8	96		-13.8±1.4
	44	16	40	2.160		5.16±0.02	3.87	0.77±0.02	0.851	325.7±3.3	123		-16.3±1.6
	44	15	41	2.150		5.16±0.04	3.90	0.77±0.01	0.851	332.3±2.4	120		-17.0±1.7
	44	13	43	2.130		5.17±0.06	3.98	0.85±0.01	0.847	331.9±2.7	98		-12.9±1.3
Annealed I phase	44	15	41	2.150		5.17±0.01	3.90	0.79±0.01	0.851	332.3±2.4	146	1.085	-26.6±2.7
2/1 phase	43	15	42	2.150	22.91	5.14±0.01	3.95	0.84±0.01	0.848	384.6±5.5	140	1.072	-24.4±2.4

III. RESULTS AND DISCUSSION

A. x-ray diffraction analysis

The diffraction spectra for the thermally stable quasicrystal and 2/1 approximant are shown in Fig. 2, along with that for the $\text{Al}_{20.5}\text{Mg}_{39.5}\text{Zn}_{40}$ as a representative of the 1/1 approximant in the (A) series of samples. All diffraction lines are very sharp and are indexed in terms of the respective phases concerned. In contrast, the x-ray-diffraction spectra for metastable quasicrystals with $x = 13, 16, 20,$ and 25 in the (B) series were rather broad and could not be sharpened by annealing. Hence, as far as metastable quasicrystals were concerned, the physical properties were measured on as-quenched $\text{Al}_x\text{Mg}_{44}\text{Zn}_{56-x}$ ($x = 13, 16, 20,$ and 25) samples.

The lattice constant can be easily calculated from the diffraction spectra for the 1/1 approximant in the (A) series and also for the 2/1 approximant. Likewise, the quasilattice constant a_R can be calculated for the quasicrystals in the (B) series. According to the projection method, the quasilattice constant a_R is interrelated with the lattice constant $a_{p/q}$ of the cubic p/q approximant through the relation

$$a_R = \frac{\sqrt{(2+\tau)}}{2(q+p\tau)} a_{p/q}, \quad (1)$$

where τ is the golden mean $\tau = (1 + \sqrt{5})/2$.^{3,4} To allow a direct comparison, we converted the lattice constants $a_{1/1}$ and $a_{2/1}$ for the 1/1 and 2/1 approximants to the corresponding quasilattice constant a_R . The results, together with the quasilattice constant for the quasicrystals, are shown in Fig. 3 as a function of the electron per atom

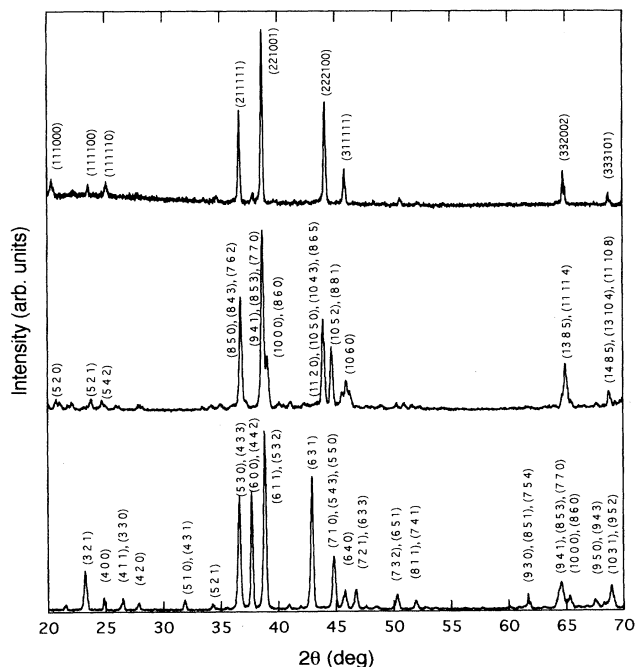


FIG. 2. X-ray diffraction spectra for (a) thermally stable icosahedral quasicrystal $\text{Al}_{15}\text{Mg}_{44}\text{Zn}_{41}$, (b) 2/1 approximant $\text{Al}_{15}\text{Mg}_{43}\text{Zn}_{42}$, and (c) 1/1 approximant $\text{Al}_{25.5}\text{Mg}_{39.5}\text{Zn}_{35}$.

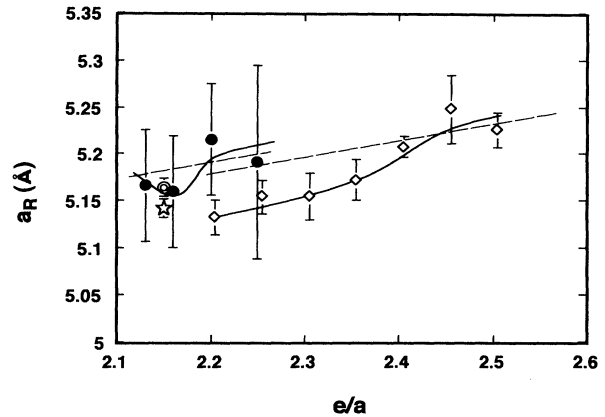


FIG. 3. Lattice constant a_R for the metastable icosahedral quasicrystals (●), thermally stable one (○), 2/1 approximant $\text{Al}_{15}\text{Mg}_{43}\text{Zn}_{42}$ (★), and 1/1 approximants (◇). The value of a_R for the approximant is derived from Eq. (1) in the text. An error bar for the metastable quasicrystal is large, since the diffraction lines are few and broad.

ratio e/a for samples in three different phases. It is noted that the error bar for the metastable quasicrystals is much larger than that for the thermally stable one because of not only the broadness in the diffraction width but also the fewer number of lines observed.

The data points for the quasicrystals containing 44 at. % Mg fall on the region consistently higher than those for the 1/1 approximants containing 39.5 at. % Mg. This reflects the fact that the atomic radius of Mg is larger than those of Al and Zn. The value for the 2/1 approximant containing 43 at. % Mg, though limited to only a single data point, is found in between them. As mentioned in the Introduction, an atomic cluster unit in all three phases under consideration is built up in common by stacking icosahedrally two different hard spheres of larger Mg and smaller Al and Zn atoms. Then, one may naturally expect the Vegard law to hold. Obviously, however, the quasilattice constant a_R does not obey a linear e/a relation for both 1/1 approximants and the quasicrystals, indicating the breakdown of the Vegard law. The lattice constant may be affected through the Fermi surface-Brillouin zone interaction. A drastic change in the slope of a_R occurs at different e/a values: $e/a = 2.4$ for the 1/1 approximants and $e/a = 2.15$ for the quasicrystals. Studies of valence band structures in the following sections will reveal that the Fermi surface-Brillouin zone matching occurs at the composition, where the slope in the lattice constant changes substantially in the respective phases.

B. Electronic structure

The XPS valence band spectra in the binding energies down to 10 eV are shown in Fig. 4 for the thermally stable quasicrystal $\text{Al}_{15}\text{Mg}_{44}\text{Zn}_{41}$ and the 1/1 approximant $\text{Al}_{25.5}\text{Mg}_{39.5}\text{Zn}_{35}$. The Zn 3d band is located in the binding energies over 9–11 eV in both cases. The overall valence band spectra in Fig. 4 are essentially identical to

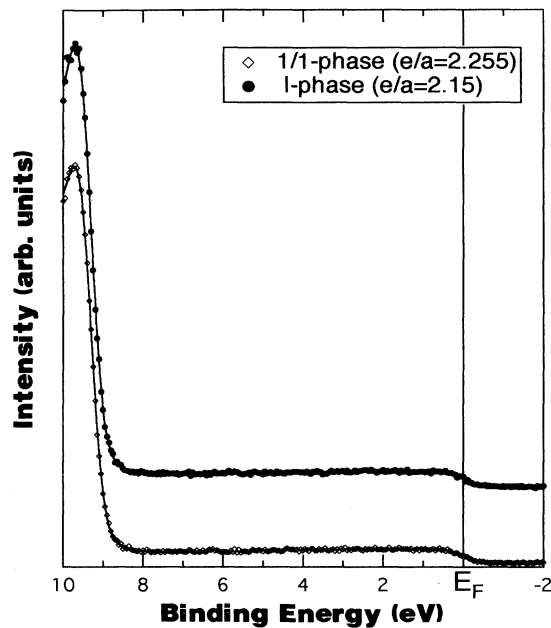


FIG. 4. XPS valence band spectra for the icosahedral quasicrystal $\text{Al}_{15}\text{Mg}_{44}\text{Zn}_{41}$ (●) and 1/1 approximant $\text{Al}_{25.5}\text{Mg}_{39.5}\text{Zn}_{35}$ (◇). The binding energy is scaled relative to the Fermi level. A huge peak below 9 eV is due to the Zn 3d band.

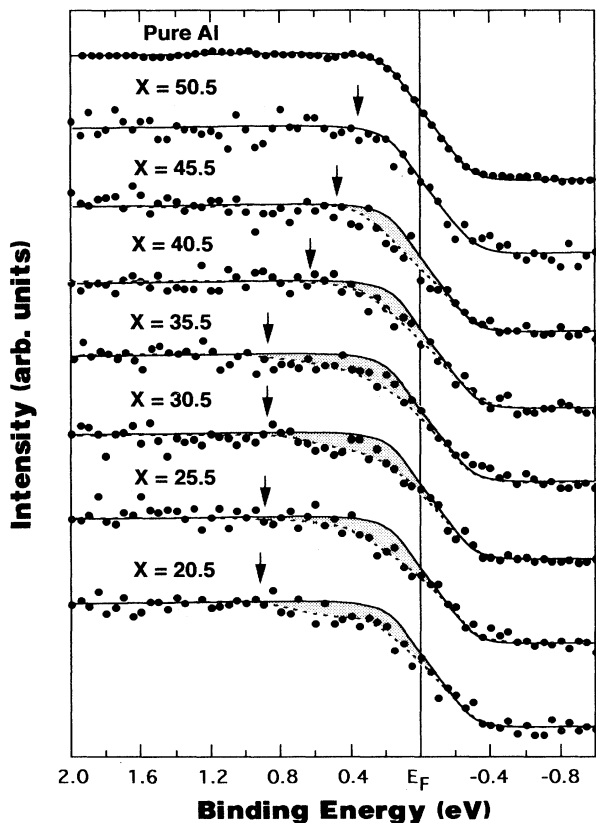


FIG. 5. XPS valence band spectra near the Fermi level for the series of 1/1 approximants $\text{Al}_{60.5-x}\text{Mg}_{39.5}\text{Zn}_x$. A spectrum for pure Al is superimposed onto each spectrum and the difference area is shown by hatches. An arrow indicates the onset of the deviation from the free-electron-like pure Al.

each other. To extract fine structures in the density of states, we accumulated the XPS signals for 2 h for all samples only in the energy range of ± 2 eV across E_F . The results for the 1/1 approximants and quasicrystals are shown in Figs. 5 and 6, respectively.

The Fermi cutoff is broadened by a combination of the instrumental resolution, thermal broadening of the Fermi distribution, and the band structure effects. All XPS spectra in the binding energies higher than about 1 eV are quite flat and structureless and cannot be distinguished from that of pure fcc Al. In order to single out the band structure effects, we superimposed the spectrum of the free-electron-like pure Al onto each spectrum of the present samples by adjusting the Fermi levels and the intensities below 1 eV to coincide with each other. A deviation emerges at the energy marked by an arrow and extends toward E_F .

We attribute the hatched area sandwiched between the data for pure Al and those for the present samples to the band structure effect associated with the pseudogap formation. It is clear that the pseudogap is essentially absent for the 1/1 approximant with $e/a=2.505$ but grows gradually with decreasing e/a in the (*A*) series of the 1/1 approximants. This means that the electronic structure of the 1/1 approximant is strongly e/a dependent: the free-electron picture holds at $e/a=2.505$ but the gap appears and grows with decreasing e/a within the range where the 1/1 approximant is stable. A decrease in e/a is brought about by replacing Al by Zn while Mg concen-

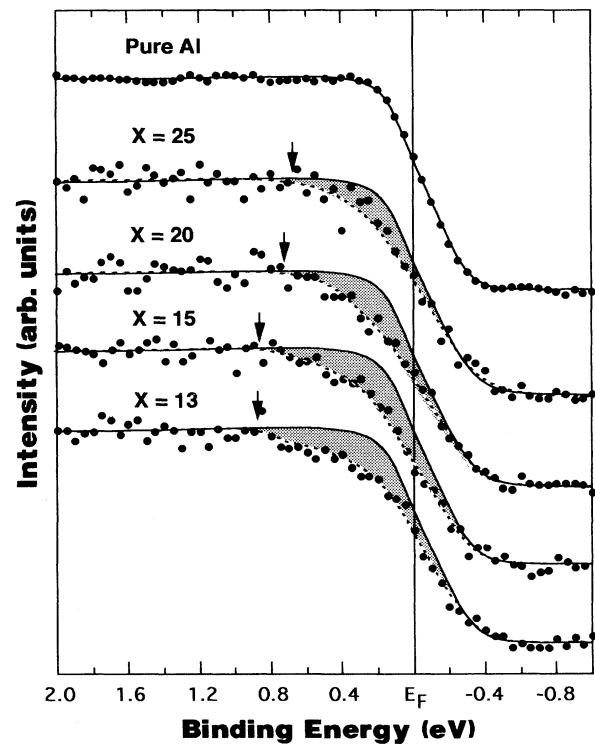


FIG. 6. XPS valence band spectra near the Fermi level for the series of the icosahedral quasicrystals $\text{Al}_x\text{Mg}_{44}\text{Zn}_{56-x}$. See the details in Fig. 5. The spectrum for the thermally stable $x=15$ sample was taken after the heat treatment.

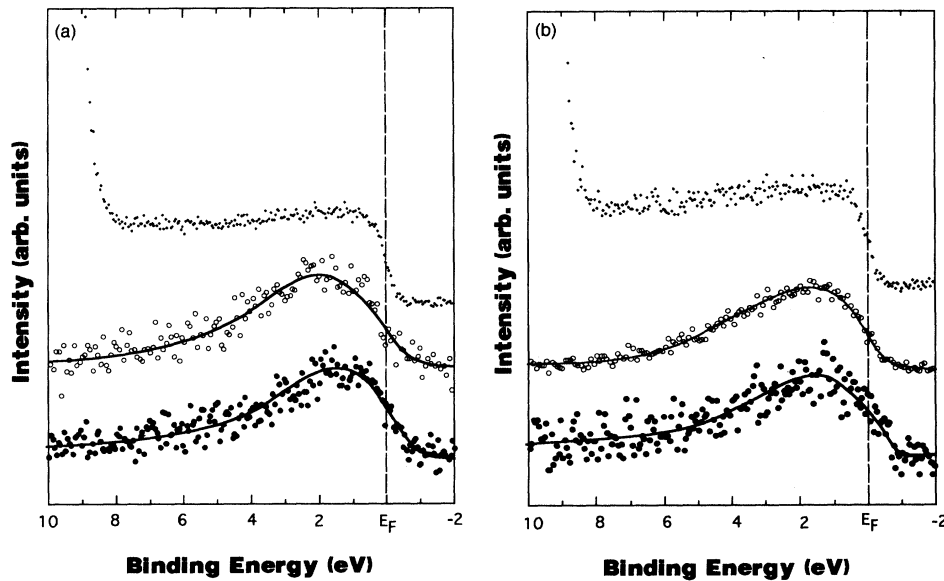


FIG. 7. Soft x-ray Al $K\beta$ (\circ) and Mg $K\beta$ (\bullet) emission spectra for (a) thermally stable icosahedral quasicrystal $\text{Al}_{15}\text{Mg}_{44}\text{Zn}_{41}$ (b) 1/1 approximant $\text{Al}_{25.5}\text{Mg}_{39.5}\text{Zn}_{35}$. The corresponding XPS valence band spectra (top) are shown for comparison.

tration is kept constant at 39.5 at. % Mg. In contrast, the pseudogap can be observed in all quasicrystals including both thermally stable and metastable ones.

The soft x-ray Al $K\beta$ and Mg $K\beta$ emission spectra were measured on both the 1/1 approximant and the thermally stable quasicrystal. The Al $K\beta$ and Mg $K\beta$ spectra reflect the Al $3p$ and Mg $3p$ electron distributions, respectively. It can be seen from Fig. 7 that both Al $K\beta$ and Mg $K\beta$ spectra are smooth without any fine structures and extend to the binding energies of about 8 eV corresponding to the bottom of the XPS valence band shown in parallel. Note here that this feature holds true, irrespective of whether the pseudogap is present or not. Therefore, the SXS spectra proved that the Al $3p$ and Mg $3p$ electrons form a free-electron-like common band without the formation of any particular atomic bonding. This is in sharp contrast to the formation of bonding and antibonding states in the Mackay-type quasicrystals like Al-Mg-Pd and Al-Pd-Re quasicrystals.²³

By summing up all spectroscopic data, we are led to conclude that the free-electron-like valence band is formed for all quasicrystals and the 1/1 approximant in the Al-Mg-Zn system and that the pseudogap is absent in the 1/1 approximant with $e/a=2.505$ but grows gradually with decreasing e/a down to 2.205 in the series of 1/1 approximants. Thus, the pseudogap may be helpful but is not a necessary condition for the stabilization of the 1/1 approximant. It is also emphasized that the electronic structure changes quite substantially as a function of e/a in the 1/1 approximant phase. In the case of the quasicrystals, the pseudogap always exists not only for thermally stable but also for metastable ones. In contrast to the 1/1 approximant, the pseudogap is now apparently needed to allow the quasicrystalline phase to exist even as a metastable state. As is shown in the inset to Fig. 1, the range where the metastable quasicrystal is formed by liquid quenching is limited to $2.13 \leq e/a \leq 2.25$, suggesting that there exists a maximum Al concentration, below which the pseudogap is formed at E_F , as is true in the 1/1 approximant.

The electronic specific-heat coefficient γ_{exp} is plotted in Fig. 8 as a function of e/a for present samples. The value of γ_{exp} for the 1/1 approximant with $e/a=2.505$ is the largest and becomes comparable to the free-electron value, if the electron-phonon enhancement factor $\lambda=0.3$ is assumed. This is consistent with the free-electron-like XPS valence band profile shown in Fig. 5. The value of γ_{exp} decreases substantially with decreasing e/a in the 1/1 approximants. This agrees again with the growth of the pseudogap with decreasing e/a , as was observed by the XPS valence band spectra. Regarding the data for the quasicrystals, we find that the value of γ_{exp} reaches the minimum at $e/a=2.15$, where the thermally stable quasicrystal and 2/1 approximant exist.

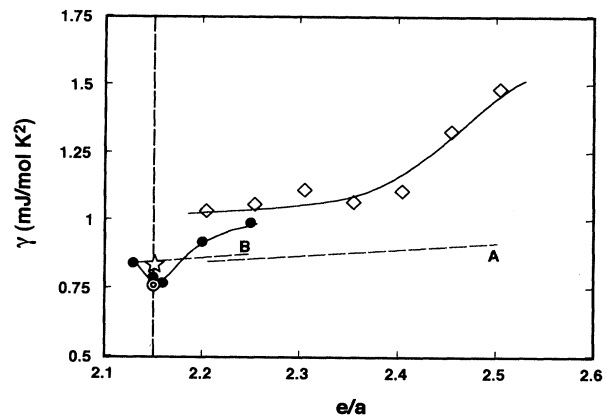


FIG. 8 Electron concentration dependence of the electronic specific-heat coefficient γ_{exp} for metastable icosahedral quasicrystals (\bullet), the thermally stable icosahedral quasicrystal $\text{Al}_{15}\text{Mg}_{44}\text{Zn}_{41}$ (\odot), 2/1 approximant $\text{Al}_{15}\text{Mg}_{43}\text{Zn}_{42}$ (\star), and 1/1 approximants (\diamond). Dashed lines A and B refer to the free-electron values for the quasicrystal and 1/1 approximant, respectively. The difference originates from that in density.

C. Electron transport properties

The Hall coefficient at 300 K is shown in Fig. 9. An agreement with the free-electron value is again reasonable for the 1/1 approximant with $e/a=2.505$. But, a downward deviation becomes substantial with decreasing e/a due most likely to the growth of the pseudogap. The Hall coefficients for metastable quasicrystals are found to be rather close to the free-electron value, in spite of the existence of the pseudogap. As shown in Fig. 9, annealing at 360°C for 1 h caused the Hall coefficient for the thermally stable quasicrystal to shift toward a more negative value and to fall close to the value for the 2/1 approximant, having the same e/a value as the thermally stable quasicrystal. It is recalled that the 2/1 approximant can be obtained after annealing and, hence is characterized by the possession of diffraction lines as sharp as those for the thermally stable quasicrystal. A good agreement in the Hall coefficient between the 2/1 approximant and the thermally stable quasicrystal suggests that the electronic structures are very similar to each other.

Figure 10 shows the e/a dependence of the resistivity, $\rho_{300\text{ K}}$, at 300 K. The value of $\rho_{300\text{ K}}$ for the 1/1 approximant with $e/a=2.505$ is only $40\ \mu\Omega\text{ cm}$. We consider this to be quite reasonable, since the free-electron picture holds in this particular sample. An increase in the value of $\rho_{300\text{ K}}$ with decreasing e/a in the 1/1 approximants is apparently brought about by a decrease in the density of states at E_F associated with the formation of the pseudogap. The resistivity for the quasicrystal is consistently higher than that for the 1/1 approximant. This certainly reflects the destruction of the translational symmetry in the quasicrystal. More important is a sharp increase in $\rho_{300\text{ K}}$ at the e/a value of 2.15, corresponding to the thermally stable quasicrystal. This is a clear demonstration that an improvement in the quasicrystallinity affects

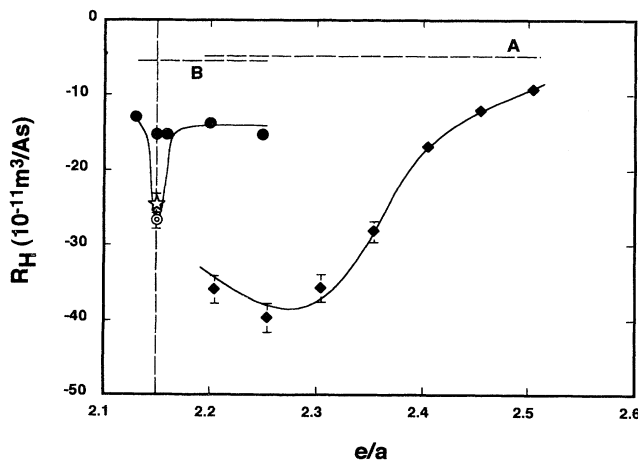


FIG. 9. Electron concentration dependence of the Hall coefficient R_H for metastable icosahedral quasicrystals (●), thermally stable icosahedral quasicrystal $\text{Al}_{15}\text{Mg}_{44}\text{Zn}_{41}$ (○), 2/1 approximant $\text{Al}_{15}\text{Mg}_{43}\text{Zn}_{42}$ (☆), and 1/1 approximants (◇). Dashed lines A and B refer to the free-electron values for the quasicrystal and 1/1 approximant, respectively.

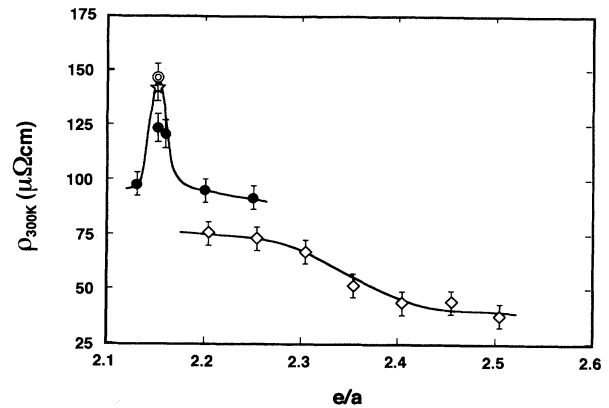


FIG. 10. Electron concentration dependence of the electrical resistivity, $\rho_{300\text{ K}}$, at 300 K for metastable icosahedral quasicrystals (●), thermally stable icosahedral quasicrystal $\text{Al}_{15}\text{Mg}_{44}\text{Zn}_{41}$ (○), 2/1 approximants $\text{Al}_{15}\text{Mg}_{43}\text{Zn}_{42}$ (☆), and 1/1 approximants (◇).

most significantly the value of $\rho_{300\text{ K}}$. It is again noted that no meaningful difference in $\rho_{300\text{ K}}$ exists between the thermally stable quasicrystal and the 2/1 approximant.

The temperature dependence of the resistivity over the range 2–300 K is shown in Fig. 11 for the 1/1 approximants, 2/1 approximant, and the thermally stable quasicrystal. All 1/1 approximants exhibit a positive temperature coefficient (TCR) over a whole temperature range in a manner consistent with the behavior of the periodic metals and alloys. However, the temperature dependence of the resistivity is essentially identical between the well-annealed thermally stable quasicrystal and the 2/1 approximant: a negative TCR dominates over a whole temperature range. This is a characteristic feature observed in nonperiodic systems having the resistivity exceeding $100\ \mu\Omega\text{ cm}$.²⁴ Hence, the 2/1 approximant behaves like a

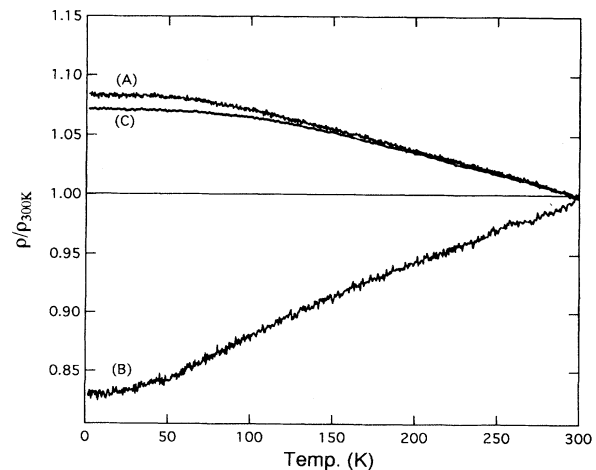


FIG. 11. Temperature dependence of the electrical resistivity for (a) thermally stable icosahedral quasicrystal $\text{Al}_{15}\text{Mg}_{44}\text{Zn}_{41}$, (b) 2/1 approximant $\text{Al}_{15}\text{Mg}_{43}\text{Zn}_{42}$, and (c) 1/1 approximant $\text{Al}_{25.5}\text{Mg}_{39.5}\text{Zn}_{35}$. The value is normalized with respect to the value at 300 K.

nonperiodic system in spite of the possession of the lattice constant of 22.9 Å and can be no longer distinguished from the thermally stable quasicrystal.^{19,20}

D. Fermi surface-Brillouin zone interaction and its effect on stability

A hypercubic lattice in the six-dimensional reciprocal space can be constructed from the hypercubic lattice in the six-dimensional real space. For example, the Γ points corresponding to the center of the first Brillouin zone in the six-dimensional reciprocal space are distributed densely everywhere, when they are projected on the three-dimensional reciprocal space. But their intensities are modulated by interference effects and the most intense ones appear quasiperiodically in the three-dimensional reciprocal space. In the absence of the translational periodicity, no reciprocal lattice vector can be defined and, therefore, the reduction of the reciprocal space to a first Brillouin zone is not possible. Instead, the quasiperiodically distributed sets of Γ points and other special points like M and X of high symmetry constitute the analog to the extended zone scheme of a crystal.

Following the extended zone scheme for the quasicrystal,²⁵ Hafner and Krajci²¹ calculated the Bloch spectral functions and obtained the dispersion relation for the 5/3 approximant to the Al-Mg-Zn quasicrystal. It consists of a series of the nearly parabolic bands, each being centered at quasiperiodically spaced intense Γ points. They pointed out that, close to the Fermi energy, highly degenerate free-electron states exist at quasiperiodically spaced wave vectors and the pseudogap appears as a result of the lifting of their degeneracies due to the electron-ion interaction. The zone formed by planes bisecting perpendicularly these wave vectors are called the “quasi-Brillouin zone” in the extended zone scheme.

The special points like Γ in the reciprocal space are responsible for the major diffraction lines shown in Fig. 2. As will be discussed below, the wave vector corresponding to the (222100) diffraction line in the quasicrystal turns out to be comparable to the Fermi diameter $2k_F$. Hence, the “quasi-Brillouin zone” mentioned above²¹ would correspond to the zone obtained by bisecting perpendicularly the equivalent wave vectors associated with the (222100) diffraction line in the quasicrystal. It is emphasized here that the quasi-Brillouin zone has many faces and is almost isotropic; thus the pseudogap is found at almost all directions of the wave vectors. It is noted further that a pair of special points with identical intensity, which are separated by a certain distance, can always be found elsewhere in the reciprocal space. The quasi-Brillouin zone formed by the sets of these special points becomes identical and is distributed quasiperiodically in the reciprocal space. This is the reason why the pseudogap opens at all wave vectors in the reciprocal space.²¹ In the discussion of the Fermi surface-Brillouin zone interaction, however, one may simply focus on one of the most intense quasi-Brillouin zones, onto which the Fermi surface is superimposed. In this way, we can discuss the Fermi surface-Brillouin zone interaction in the quasicrystal on the same footing as in the approximant crystal, to

which the ordinary extended zone scheme holds.

As mentioned in the Introduction, the diffraction peak positions in the 1/1 approximant differ quite substantially from those in the quasicrystal. This means that the Brillouin zone affects the electronic structure at different electron concentrations between these two structures. The Fermi surface-Brillouin zone interaction in both quasicrystal and approximants may be conveniently discussed, using the matching condition between the Fermi wave number $2k_F$ and the wave vector \mathbf{K}_n responsible for the major diffraction peaks. By inserting the measured density d listed in Table I and an average atomic weight A into the free-electron equation $2k_F = 5.226(e/a)^{1/3}(d/A)^{1/3}$, one can easily find that the $2k_F$ value in $2.1 < e/a < 2.6$ is confined in the range $3.05\text{--}3.25 \text{ \AA}^{-1}$ for both quasicrystals and 1/1 approximants. For the quasicrystal, the only \mathbf{K}_n value associated with the (222100) diffraction line is found in this range. In the case of the 1/1 approximant, the reciprocal lattice vectors associated with (631), (543)+(710)+(550), and (640) planes are possible candidates. Among them, (631), (543), and (710) reciprocal lattice vectors originate from the splitting of the 60-fold (222100) reflections of the icosahedral phase. But, the reciprocal lattice vector \mathbf{K}_{631} is excluded, since it is too short to coincide with $2k_F$ in the given e/a range. The magnitude of the relevant wave vector, K_n , for the 2/1 approximant can be obtained only at $e/a = 2.15$. Both K_n and $2k_F$ values thus obtained are plotted in Fig. 12 as a function of e/a for all three phases.

As is clear from Fig. 12, the $2k_F$ line crosses the K_n curve at $e/a = 2.15$ for the quasicrystal as well as the 2/1 approximant and at 2.3–2.4 for the 1/1 approximant. In the previous sections, we have shown that the pseudogap at the Fermi level becomes the deepest at $e/a = 2.15$ for the thermally stable quasicrystal, whereas it grows with decreasing e/a below 2.5 for the 1/1 approximant. Furthermore, the great similarity of the electronic structure and electron transport properties is emphasized between

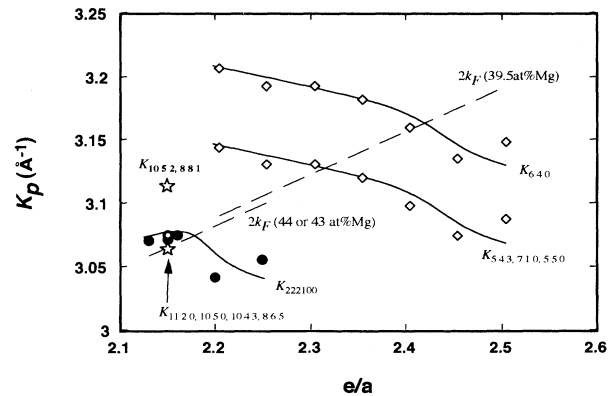


FIG. 12. The magnitude of the reciprocal lattice vector K_n and the Fermi diameter $2k_F$ as a function of e/a for the icosahedral quasicrystals, 2/1, and 1/1 approximants. The $2k_F$ value is calculated in the free-electron model by inserting e/a and density d into the equation $2k_F = \{3\pi^2(e/a)dN_A/A\}^{1/3}$, where N_A is the Avogadro number and A is an average atomic weight.

the thermally stable quasicrystal and the 2/1 approximant, both being stabilized at the electron concentration of 2.15. Obviously, observed electronic structures and electron transport properties can be consistently accounted for in terms of the $2k_F = K_n$ matching condition shown in Fig. 12 for all three relevant phases. This allows us to call them the Hume-Rothery electron phases.²⁶ As only one puzzling behavior, we point to the case where $2k_F$ exceeds K_n and, hence, the density of states anomaly associated with K_n would be shifted below E_F . This situation is realized in the 1/1 approximant with $e/a = 2.505$. However, the XPS valence band spectrum shown in Fig. 5 indicates no anomaly below E_F within the accuracy of the measurements. One possible reason for this is that the effect is too weak to be observed when the Al concentration is high.

Finally, we discuss the relative stability of the quasicrystals and two different approximants. As has been emphasized, the 1/1 approximant or the Frank-Kasper phase is known to exist along a constant 39.5 at. % Mg concentration line. We revealed that the pseudogap is essentially absent, when the electron concentration is above $e/a = 2.50$ or 50 at. % Al in the 1/1 approximant. This means that, at least at this composition, the electronic energy does not contribute to the stabilization of the 1/1 approximant. Instead, a constant size ratio of a larger Mg atom over smaller Al and Zn atoms suggests that the size factor contribution plays a more important role in stabilizing the 1/1 approximant along this particular concentration line. As a matter of fact, the most favorable packing ratio for two different hard spheres is believed to be realized in the $(\text{Al,Zn})_{49}\text{Mg}_{32}$ Frank-Kasper lattice.⁸ Hence, the composition ratio of larger Mg atoms over smaller Al and Zn atoms, $x_{\text{Mg}}/(x_{\text{Al}} + x_{\text{Mg}})$, equal to 0.65 should be very important in stabilizing the 1/1 approximant.

The pseudogap appears in the 1/1 approximant, when the e/a value or the Al concentration is lowered. Now the electronic energy is lowered by forming the pseudogap and begins to contribute to stabilizing the 1/1 approximant. From the phase diagram, however, we know that the 1/1 approximant loses its stability relative to the C14-Laves phase when the e/a is lowered below 2.2. We consider that neither higher-order approximants nor a thermally stable quasicrystal can be formed along the 39.5 at. % Mg line, because the composition ratio of 0.65 would favor only the size of an icosahedral cluster present in the 1/1 approximant and the icosahedral cluster larger than that in the 1/1 approximant would require a different Mg concentration.

We found in this experiment that the 2/1 approximant and thermally stable quasicrystal can be stabilized at specific compositions of 43 and 44 at. % Mg, respectively, while keeping the electron concentration to 2.15. As is clear from all experimental evidence shown in this experiment, the electron concentration of 2.15 is critically needed for the icosahedral quasicrystal and 2/1 approximant. Thus, the composition in Mg concentration can vary along the $e/a = 2.15$ line to reach higher-order approximants and icosahedral quasicrystal. The composition ratio $x_{\text{Mg}}/(x_{\text{Al}} + x_{\text{Zn}})$ increases from 0.65 in the 1/1 ap-

proximant to 0.75 in the 2/1 approximant and 0.78 in the icosahedral quasicrystal. This suggests that a packing balance of a larger Mg atom over smaller Al or Zn atoms in building up the 1/1 approximant collapses when the ratio deviates from 0.65. The 2/1 approximant possessing an icosahedral cluster larger than that in the 1/1 approximant is stabilized when the ratio reaches 0.75 along the $e/a = 2.15$ line. Further increase in the ratio up to 0.78 along the $e/a = 2.15$ line is apparently needed to reach the icosahedral quasicrystal. The stability of the three competing phases, icosahedral quasicrystal, 2/1, and 1/1 approximants in the Al-Mg-Zn alloy system is, therefore, decided by the Hume-Rothery mechanism: electron concentration and size factor.²⁶

Henley and Elser⁶ pointed out that the icosahedral quasicrystal would possess the composition of $(\text{Al,Zn})_{0.629}\text{Mg}_{0.371}$, provided that smaller Al and Zn occupy all Z12 or Z13 coordination number sites, while the larger Mg atoms are all Z14, Z15, or Z16 sites. This is obviously not consistent with our observation. However, the Mg atoms may be easily substituted for Al/Zn in the Z13 sites, as they also suggested. Our ratio of 0.78 can be obtained, if 75% of Al/Zn atoms in the Z13 are replaced by Mg atoms. Further work is of great interest in pursuing the Mg concentration dependence of the icosahedral cluster size in the Al-Mg-Zn alloy system.

IV. CONCLUSION

We revealed the existence of a thermally stable quasicrystal $\text{Al}_{15}\text{Mg}_{44}\text{Zn}_{41}$ and the 2/1 approximant $\text{Al}_{15}\text{Mg}_{43}\text{Zn}_{42}$, both characterized by the possession of $e/a = 2.15$, whereas the 1/1 approximant exists over a wide electron concentration range $2.2 < e/a < 2.5$ in the Al-Mg-Zn system. All properties we measured are consistent with the conclusion that the electronic structure and the resulting electron transport properties of icosahedral quasicrystals are substantially different from those of the 1/1 approximant but are essentially the same as those of the 2/1 approximant. The valence band structure in these three phases can be described by the free-electron picture with the formation of the pseudogap resulting from interaction with the zone planes associated with the (222100) planes in the quasicrystal and those resulting mainly from its splitting in the 1/1 and 2/1 approximants. Their relative stability is decided by the Hume-Rothery mechanism: electron concentration or $2k_F = K_n$ criterion, which measures the lowering of the electronic energy due to the pseudogap formation and the size factor or the composition ratio $x_{\text{Mg}}/(x_{\text{Al}} + x_{\text{Zn}})$ for a larger Mg atom over smaller Al and Zn atoms. Hence, they can all be regarded as being typical of Hume-Rothery electron phases.

ACKNOWLEDGMENT

We are very grateful to Professor K. Niizeki, Tohoku University, for valuable discussions on the extended zone scheme for the quasiperiodic lattice.

- ¹D. Shechtman, I. Blech, D. Gratias, and J. W. Cahn, *Phys. Rev. Lett.* **53**, 1951 (1984).
- ²S. J. Poon, *Adv. Phys.* **41**, 303 (1993).
- ³V. Elser, *Phys. Rev.* **32**, 4892 (1985); *Acta Crystallogr. A* **42**, 36 (1986).
- ⁴V. Elser and C. L. Henley, *Phys. Rev. Lett.* **55**, 2883 (1985).
- ⁵T. Fujiwara, *Phys. Rev. B* **40**, 942 (1989).
- ⁶C. L. Henley and V. Elser, *Philos. Mag. B* **53**, L59 (1986).
- ⁷T. Fujiwara and T. Yokokawa, *Phys. Rev. Lett.* **66**, 333 (1992).
- ⁸G. Bergman, J. L. T. Waugh, and L. Pauling, *Acta Crystallogr.* **10**, 254 (1957).
- ⁹P. Ramachandrarao and G. V. S. Sastry, *Pramana* **25**, L255 (1985).
- ¹⁰H. Yamane, K. Kimura, T. Shibuya, and S. Takeuchi, *Mater. Sci. Forum* **22-24**, 539 (1987).
- ¹¹T. Matsuda, I. Ohara, H. Sato, S. Ohashi, and U. Mizutani, *J. Phys. Condens. Matter* **1**, 4087 (1989).
- ¹²A. Niikura, A. P. Tsai, N. Nishiyama, A. Inoue, and T. Masumoto, *Mater. Sci. Eng.* **A181-A182**, 1387 (1994).
- ¹³T. Takeuchi, S. Murasaki, A. Matsumuro, and U. Mizutani, *J. Non-Cryst. Solids* **156-158**, 914 (1993).
- ¹⁴U. Mizutani, T. Takeuchi, and T. Fukunaga, *Mater. Trans. JIM* **34**, 102 (1993).
- ¹⁵T. Takeuchi, Y. Yamada, T. Fukunaga, and U. Mizutani, *Mater. Sci. Eng.* **A181-A182**, 828 (1994).
- ¹⁶U. Mizutani, A. Kamiya, T. Matsuda, K. Kishi, and S. Takeuchi, *J. Phys. Condens. Matter* **3**, 3711 (1991).
- ¹⁷E. Belin and A. Traverse, *J. Phys. Condens. Matter* **3**, 2157 (1991).
- ¹⁸K. Edagawa, N. Naito, and S. Takeuchi, *Philos. Mag. B* **65**, 1011 (1992).
- ¹⁹U. Mizutani, A. Kamiya, T. Fukunaga, and T. Matsuda, *Proceedings of the China-Japan Symposium on Quasicrystals*, edited by K. H. Kuo and T. Ninomiya (World Scientific, Singapore, 1991), p. 248.
- ²⁰U. Mizutani, T. Matsuda, Y. Itoh, K. Tanaka, H. Domae, T. Mizuno, S. Murasaki, Y. Miyoshi, K. Hashimoto, and Y. Yamada, *J. Non-Cryst. Solids* **156-158**, 882 (1993).
- ²¹J. Hafner and M. Krajci, *Phys. Rev. B* **47**, 11 795 (1993).
- ²²M. Windisch, M. Krajci, and J. Hafner, *J. Phys. Condens. Matter* **6**, 6977 (1994).
- ²³U. Mizutani, Y. Yamada, T. Takeuchi, K. Hashimoto, E. Belin, A. Sadoc, T. Yamauchi, and T. Matsuda, *J. Phys. Condens. Matter* **6**, 7335 (1994).
- ²⁴U. Mizutani, *Phys. Status Solidi B* **176**, 9 (1993).
- ²⁵K. Niizeki and T. Akamatsu, *J. Phys. Condens. Matter* **2**, 2759 (1990).
- ²⁶T. B. Massalski and U. Mizutani, *Prog. Mater. Sci.* **22**, 151 (1978).
- ²⁷J. B. Clark, *Trans. Am. Soc. Met.* **53**, 295 (1961).